

Electronic structure and optical absorption of C90 fullerene isomers

© A.I. Murzashev, M.Yu. Kokurin, A.P. Zhumanazarov, S.K. Paymerov

Mari State University,
424000 Yoshkar-Ola, Russia
e-mail: nanotubes59@mail.ru

Received October 22, 2021

Revised December 25, 2021

Accepted December 26, 2021

The energy spectra and optical absorption spectra of isomers Nos. 1, 6, 16 and 46 of fullerene C90 are calculated. Due to the comparison of theoretical and experimental optical absorption spectra, three previously synthesized isomers of C90 fullerene have been identified. The calculations are carried out within the framework of the developed approach, taking into account the intra-node Coulomb interaction of π -electrons, which plays a crucial role in the formation of the electronic and optical properties of fullerenes.

Keywords: fullerene, intra-node Coulomb interaction, Hubbard model, Coulomb integral, energy spectrum, selection rules, optical absorption spectrum.

DOI: 10.21883/EOS.2022.06.54717.2828-21

1. Introduction

Fullerenes were discovered more than 35 years ago. Despite the long time that passed from the moment of their discovery, fullerenes still arouse continued interest among researchers. This is primarily due to their unique physical properties. In fullerenes, each atom of carbon is bound with another three atoms of carbon. As a result, three out of four carbon valence electrons are hybridized and form rigid bonds between neighboring atoms. The fourth, non-hybridized electron remains unengaged in these bonds. Due to overlapping wave functions of neighboring atoms the above-mentioned electrons form so-called π -band, correspondent valence state is called sp^2 -hybridized state. It is important to note, that the boundary between the vacant and occupied states in fullerenes lies in the energy region of π -band.

In [1], it was shown that carbon systems with sp^2 -hybridization are characterized by strong intrasite Coulomb interaction (ISCI) of π -electrons, and the Coulomb integral can be as high as $U \sim 10$ eV. This requires significantly different approaches to studying the electron structure of fullerenes and carbon nanotubes (CNT) as compared with those that are often used now. With high values of the Coulomb interaction integral, strong Coulomb correlations start to play an important role in the electron subsystem [2]. In particular, when $U > W$, where W is width of the π -band, the system becomes unstable in terms of metal–dielectric transition [3,4]. Nevertheless, with reasonable assumptions, researchers succeeded in interpreting the experimental data in models where ISCI is not taken into account at all. These interpretations use both the simple Hückel approximation, and different methods of electron density functional. This paradoxical situation can be explained by the considerations described below.

One of the first experimental study of carbon systems in sp^2 -hybridized state is the work of Sagawa [5], where Auger spectroscopy method is used to measure the density of electron states. Width of the occupied part of π -electron band turned out to be ~ 5.8 eV. Taking into account the data of Sagawa and the results of Wallace [6], according to which in the carbon plane, in an approximation of strong binding, without taking into account the ISCI, width of π -electron band is $\sim 6|B|$, a conclusion can be made that $|B| \sim 2.0$ eV. Here B is the integral of wave function overlap of π -electrons between neighboring sites. Further refinement of this parameter on the basis of analysis of experimental optical absorption spectra (OAS) of carbon nanosystems without taking into account the ISCI yielded an estimate of $B \sim 2.6$ eV [7–9].

After all, within this model without taking into account the ISCI, it is possible to obtain a relatively experiment-matching representation of electron and optical properties of fullerenes and other carbon nanosystems. However, further studying of carbon nanosystems resulted in emergence of a number of contradictions between experimental and theoretical data, which suggests the incomplete adequacy of this model. According to results of Dresselhaus team obtained without taking into account Coulomb interaction and with an overlap integral of $B = -2.6$ eV [10], the type of conductivity of carbon CNTs should be critically dependent on their chirality indices. If the difference between these indices is a multiple of three, then CNTs should be conductors, otherwise they should be dielectric materials or semiconductors. However, direct measurements of the electrical resistance of CNTs do not indicate such an unambiguous correlation [11]. Contradictions between the theoretical data obtained within this model, and the experimental results also arise during investigations of fullerenes. For example, according to this model

the gap between occupied and vacant electron states (HOMO-LUMO) in C₇₄ fullerene should be ~ 0.01 eV [12], but there is no experimental confirmation for it. The same situation is observed when comparing the results of calculation by the method of electron density functional with the experimental data. Thus, in [13] the energy spectrum and optical absorption spectrum of isomer № 3 of fullerene C₈₂ (the number is referred to in accordance with An Atlas of Fullerenes [14]) were calculated using standard TD-DFT method without taking into account the ISCI. Authors of [13] succeeded in obtaining a qualitative match with experimental data only due to an artificial shift of calculated values of energy levels by ~ 0.3 eV.

Based on the above said considerations, we result in the need to take into account the ISCI in fullerenes and CNTs. This task can be solved correctly within the Hubbard model [2]. Unfortunately, it is difficult to obtain explicit accurate solutions for non-trivial atom configurations within this model. In this context, it should be noted the accurate solution for an infinite chain of atoms [15], which is not applicable for description of fullerenes and CNTs. The diagram method of [16] and different decoupling methods of [17] make it possible to describe a number of interesting phenomena, that are observed in transition metals and high-temperature superconductors in cuprates. Note that methods of [16,17] are only applicable in the extreme case of $U \gg W$, which is evidently unacceptable for CNTs and fullerenes, where $U \sim 10.0$ eV, and $W \sim 6.0$ eV, as shown below. The task becomes simpler if we consider the system at temperatures of ~ 300 K. As known, the processes with electron spin-flip can be neglected at these temperatures. Then, the processes related to ISCI and the processes related to intersite hopping of π -electrons can be considered separately. This idea is implemented within the approximation of static fluctuations (ASF) [18–20]. Here it is possible to accurately take into account the hopping of π -electrons between neighboring sites and their ISCI. It is assumed that the effects related to interference of these two processes are insignificant.

Previously we have investigated CNTs with different chirality and fullerenes C₆₀, C₇₀, C₇₂, C₇₄, C₈₀, C₈₄ and C₉₆ within the Hubbard model under the above-specified conditions. Energy spectra of π -electrons were calculated in ASF, i.e. taking into account the ISCI. The calculated OAS of investigated systems match the experimental spectra with a good quality level [21–29].

The calculations performed in the above-mentioned studies expectedly show that ISCI results in division of each energy level of π -electrons into two levels. This is a consequence of the fact that energies of states at single- and double-occupations of a site by an electron differ from each other by U . Due to this, the band of π -electrons is divided into two Hubbard subbands, each with a width of $W \sim 6|B|$. The bottom Hubbard subband corresponds to states with single-occupation of site by π -electron, the top subband corresponds to double-occupations. The distance between

corresponding levels of bottom and top Hubbard subbands is approximately equal to U . If $U > 6|B|$, then there is a gap of $\Delta \approx U - 6B$ in the energy spectrum. In the ground state, the bottom Hubbard subband is completely occupied, while the top subband is vacant. Taking into account, that according to results of [6] width of the occupied π -band is ~ 5.8 eV, we get $B \approx -1.0$ eV. Since in the fullerene C₆₀ the HOMO-LUMO ~ 1.0 eV, then the Coulomb interaction integral in fullerenes should be $U \sim 7.0$ eV. From here, taking into account the results of [1,2] [21–29], it follows that carbon nanosystems, fullerenes and CNTs can be described correctly within the Hubbard model with the following parameters: $B \sim -1.0$ eV and $U \sim 7.0$ eV. The difference between the Coulomb interaction integral of $U \sim 7.0$ eV and results of [1] is explained by screening of ISCI, the Coulomb interaction of π -electrons in neighboring sites [30]. For the π -electron band width our analysis yields a value of $\sim 6|B| + U$, which is close to the experimentally observed value of ~ 14 eV.

It is said in the above that results of experiments, in particular those related to OAS, for many fullerenes can be explained within reasonable assumptions both within the models without taking into account the ISCI, with $B = -2.6$ eV, and within ASF for the Hubbard model, i.e. with taking into account the ISCI. In this context, it is of interest to perform a comparative study of electron structure and OAS within these two models for different fullerenes. The purpose of this work is precisely this study of electron structure and optical properties of isomers of fullerene C₉₀.

First isomers of fullerene C₉₀ were synthesized in early 90s of last century. In [31] different isomers of fullerenes C₆₀, C₇₀, C₇₆, C₇₈, C₈₂, C₈₄, C₉₀ and C₉₆ were obtained from the carbon soot produced by arc heating. Currently, when searching for and identifying stable fullerenes, researchers rely on the „isolated-pentagon rule“ (IPR). According to this rule, the most stable isomers are those where each pentagon is surrounded by hexagons. According to [14], fullerene C₉₀ has 46 such isomers. Among them one isomer has D_{5h} symmetry, seven isomers have C_{2v} symmetry, six isomers have C_s symmetry, sixteen isomers have C_1 symmetry, and sixteen isomers have C_2 symmetry. We have calculated energy spectra of all these isomers of fullerene C₉₀. In this study we report the results related to isomers №№ 1, 6, 16 and 46. Our choice is grounded on the fact that there are experimentally obtained OAS spectra for these isomers. For comparison with experimental data, the calculations were performed within two models: the Hückel approximation with overlap integral of $B = -2.6$ eV, and the Hubbard model taking into account the ISCI. The method of calculation in ASF is described in detail in our work [27] (also, see [21–29]). To avoid overloading of the paper, we omit this description here and refer the reader to the listed works.

Table 1. Permitted dipole transitions for group C_{2v}

C_{2v}	A_1	A_2	B_1	B_2
A_1	+	–	+	+
A_2	–	+	+	+
B_1	+	+	+	–
B_2	+	+	–	+

Table 2. Permitted dipole transitions for group D_{5h}

D_{5h}	A'_1	A'_2	E'_1	E'_2	A''_1	A''_2	E''_1	E''_2
A'_1	–	–	+	–	–	+	–	–
A'_2	–	–	+	–	+	–	–	–
E'_1	+	+	–	+	–	–	+	–
E'_2	–	–	+	+	–	–	–	+
A''_1	–	+	–	–	–	–	+	–
A''_2	+	–	–	–	–	–	+	–
E''_1	–	–	+	–	+	+	–	+
E''_2	–	–	–	+	–	–	+	+

2. Symmetry and selection rules for fullerenes of point groups C_1 , C_2 , C_s , C_{2v} , D_{5h}

To built up OAS of a fullerene, it is necessary to take into account the selection rules conditioned by the symmetry of the point group of this fullerene. For this purpose, symmetry groups were studied that include isomers of fullerene C_{90} , meeting the IPR, and selection rules were found for dipole optical transitions. This section includes a brief description of the obtained results.

For fullerenes with low-symmetry groups of symmetry (C_1 , C_2 , C_s) all transitions between energy levels are permitted. These groups can be described as follows [32].

1) Group C_1 is a trivial group. It is an Abelian group and has the only irreducible representation (A).

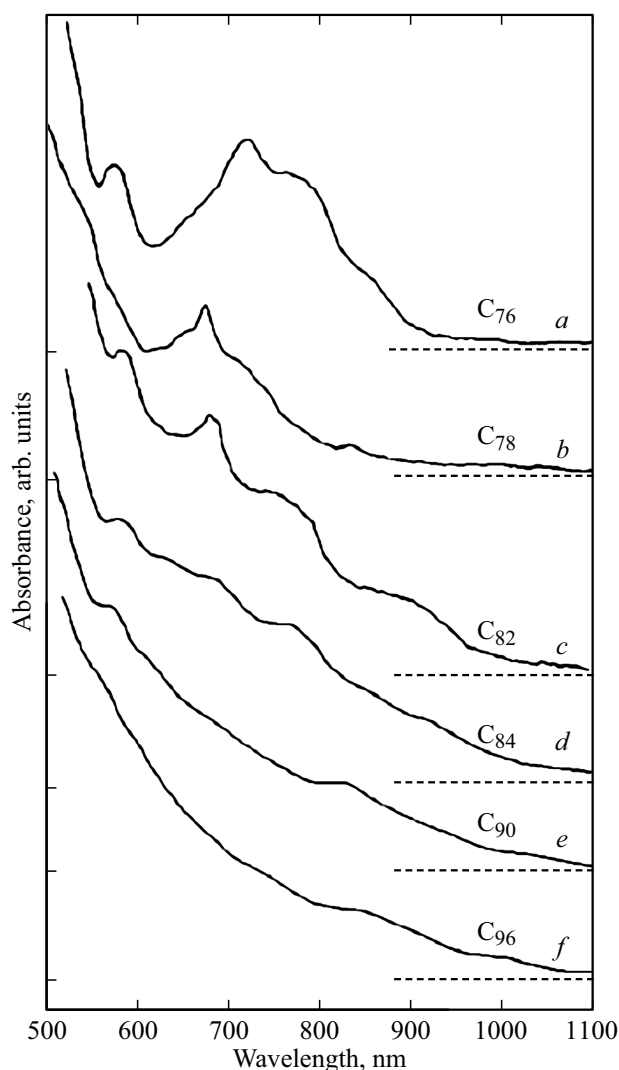
2) Point group C_2 contains two operations of symmetry: E — identity transformation, C_2 — twofold axis of symmetry. It is an Abelian group that has two irreducible representations (A and B).

3) Point group C_{1s} contains two operations of symmetry: E — identity transformation, $\sigma = \sigma_h$ — mirror plane of symmetry that can be considered horizontal. It is an Abelian group that has two irreducible representations (A' and A'').

4) Point group C_{2v} contains four operations of symmetry: E — identity transformation, $C_2 = C_2(z)$ — twofold axis of symmetry, $\sigma_v = \sigma_v(xz)$ — the first mirror plane of symmetry (xz), $\sigma'_v = \sigma_v(yz)$ — the second mirror plane of symmetry (yz). It is an Abelian group that has four irreducible representations (A , A_2 , B_1 , B_2).

5) Point group D_{5h} contains the following operations of symmetry: E — identity transformation, C_5 — the main axis of symmetry of the 5-th order, $5C'_2$ — five twofold axes of symmetry orthogonal to the main axis, σ_h — horizontal mirror plane crossing the main axis of symmetry, $5\sigma_v$ — five vertical mirror planes parallel to the main axis of symmetry, S_5 — improper rotation axis of the 5-th order. This is not an Abelian group that has eight irreducible representations (A'_1 , A'_2 , E'_1 , E'_2 , A''_1 , A''_2 , E''_1 , E''_2).

Irreducible representations for fullerenes of point groups C_{2v} and D_{5h} are identified using Maple software. Then, using the selection rules for permitted dipole transitions (Tables 1 and 2), we obtain OAS of fullerenes that belong to these groups of symmetry.

**Figure 1.** Experimental OAS of synthesized fullerenes [33].

3. Energy spectrum and optical absorption spectrum of isomer № 6 of fullerene C_{90}

Fullerene C_{90} , as mentioned above, was obtained for the first time as early as in 1992 [31]. Optical absorption spectra of isomers C_{76} , C_{78} , C_{82} , C_{84} , C_{90} and C_{96} covered in

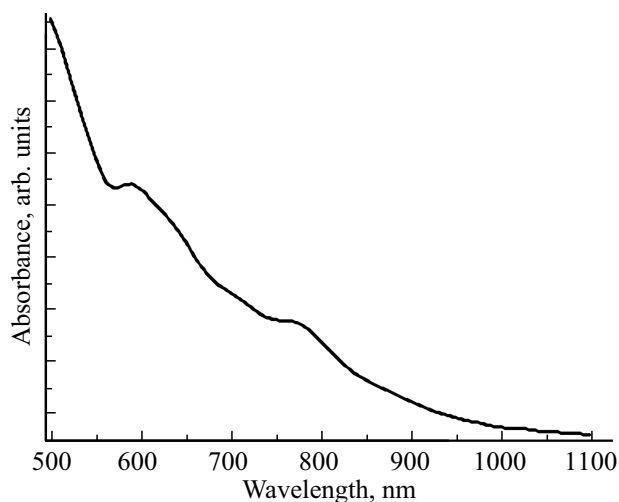


Figure 2. Optical absorption spectrum of isomer № 6 calculated within the Hubbard model with $U = 7.48$ eV, $B = -1.05$ eV.

this study are shown in Fig. 1. Based on the comparison of curves, authors of [31] conclude the following: „it can be seen that the absorption threshold shifts to the red wavelength region by increasing the number of carbon atoms“. This conclusion can be easily explained within our model taking into consideration the ISCI. The absorption threshold is defined by the HOMO-LUMO gap. This gap is defined as $\Delta = U - W$, where W is width of the Hubbard subband. Following [5,6] and results of our calculations of energy spectra of fullerenes C_{60} – C_{96} , we conclude that W increases with increase in the number of atoms of fullerene from ~ 5.0 eV for C_{60} up to ~ 5.8 eV for C_{96} , achieving maximum value of $6|B|$ in the graphite plane and CNT. Taking into account that $|B| \sim 1.0$ eV and $U \sim 7.0$ eV, the HOMO-LUMO gap decreases with increase in the number of atoms, achieving its minimum value of ~ 1.0 eV. As a result, the absorption threshold shifts to the red wavelength region achieving its maximum of ~ 1200 nm. The above said is true for fullerenes with low symmetry where all transitions from the bottom Hubbard subband to the top subband are permitted. In fullerenes with high symmetry, due to the fact that transitions between states with an energy difference equal to HOMO-LUMO ~ 1.0 eV may be prohibited, the absorption edge may be significantly lower than 1200 nm.

To identify the isomer obtained in [31], we have compared the curve „e“ shown in Fig. 1 (taken from [3]) with optical absorption spectra of isomers obtained within the Hubbard model. The comparison has shown that the best match between experimental and theoretical OAS is observed for the OAS of isomer № 6 with C_2 symmetry at the following parameters of the Hubbard model: $B = -1.05$ eV and $U = 7.48$ eV. Optical absorption spectrum of isomer № 6 (C_2) of fullerene C_{90} at these values of parameters is shown in Fig. 2. It can be seen from Fig. 2, that the experimental curve has maxima at 570 and 840 nm, while

Table 3. Energy spectrum of isomer № 6 at $U = 7.48$ eV, $B = -1.05$ eV

–6.890	–4.009	0.5900	3.471
–6.746	–3.645	0.7342	3.835
–6.711	–3.577	0.7691	3.903
–6.701	–3.464	0.7792	4.016
–6.454	–3.402	1.026	4.078
–6.428	–3.131	1.052	4.349
–6.401	–2.984	1.079	4.496
–6.358	–2.844	1.122	4.636
–6.320	–2.760	1.160	4.720
–6.039	–2.739	1.441	4.741
–6.039	–2.652	1.441	4.828
–6.003	–2.568	1.477	4.912
–5.942	–2.550	1.538	4.930
–5.879	–2.518	1.601	4.962
–5.836	–2.442	1.644	5.038
–5.808	–2.419	1.672	5.061
–5.577	–2.381	1.903	5.099
–5.563	–2.298	1.917	5.182
–5.483	–2.290	1.997	5.190
–5.407	–2.260	2.073	5.220
–5.379	–2.220	2.101	5.260
–5.335	–2.173	2.145	5.307
–5.320	–2.139	2.160	5.341
–5.238	–2.082	2.242	5.398
–5.177	–2.039	2.303	5.441
–5.008	–1.968	2.472	5.512
–4.989	–1.900	2.491	5.580
–4.943	–1.855	2.537	5.625
–4.904	–1.798	2.576	5.682
–4.902	–1.722	2.578	5.758
–4.823	–1.720	2.657	5.760
–4.782	–1.580	2.698	5.900
–4.746	–1.530	2.734	5.950
–4.711	–1.467	2.769	6.013
–4.652	–1.362	2.828	6.118
–4.638	–1.361	2.842	6.119
–4.558	–1.311	2.922	6.169
–4.544	–1.191	2.936	6.289
–4.539	–1.020	2.941	6.460
–4.525	–1.008	2.955	6.472
–4.433	–0.9834	3.047	6.497
–4.401	–0.9372	3.079	6.543
–4.323	–0.8406	3.157	6.639
–4.238	–0.8284	3.242	6.652
–4.117	–0.8245	3.363	6.655

the theoretical curve has corresponding maxima at 590 and 790 nm. Taking into account measurement errors and errors of the model, a conclusion can be made that a sufficiently good qualitative match is observed. Energy spectrum of the isomer under consideration is shown in Table 3. It can be seen that the energy spectrum is composed of 180 energy levels: the bottom Hubbard subband (negative energies) has 90 levels, the top subband has 90 levels (positive energies). Width of each subband is ~ 6.06 eV, the HOMO-LUMO gap is 1.41 eV.

HOMO-LUMO = 1.41 eV corresponds to an absorption edge of ~ 880 nm. It is mentioned above that in systems with the symmetry group C_2 all transitions are permitted. Therefore the OAS shown in Fig. 2 is formed by all the 8100 transitions between 90 levels from the bottom Hubbard subband to 90 levels of the top Hubbard subband. Thus, each absorption band in the curve of Fig. 2 is formed by a large number of transitions between different levels. The OAS curve is defined by the following expression:

$$In(\lambda) \sim \sum_{i,k} M_k M_i \frac{\delta}{(E_k - E_i - \frac{1243}{\lambda})^2 + \delta^2}. \quad (1)$$

Here M_k, M_i — degeneracy order of energy levels, δ — phenomenological parameter, that characterizes decay of the levels, λ — wavelength of the electromagnetic radiation. Summing up in (1) is performed over all k levels of the top subband and over i levels of the bottom subband. Each term in the sum in (1) is a Gaussian curve having its maximum at $\lambda_{\max} = 1243 \cdot (E_k - E_i)$. In (1) the energies of E_k, E_i levels are measured in eV, and wavelength λ is measured in nm.

It is evident that the OAS curve has maxima at the regions, where Gaussian curves are located more densely. A few words about absorption edge. Figure 3 shows three Gaussian curves on the background of OAS that contribute to the OAS near the absorption edge. For illustrative purposes intensities of these curves are 10 times zoomed. These curves correspond to transition between levels with energy differences of 1.415, 1.418 and 1.431 eV. They are responsible for absorption of electromagnetic waves with wavelengths of 878, 877 and 868 nm (below, in Fig. 5 the curves with $\lambda_{\max} = 878$ and 877 nm are combined). There are no any other transitions in this wavelength region except for the above-mentioned transitions. Nonzero absorption intensity in the region under consideration is defined by the sum of „tails“ of a large number of Gaussian curves corresponding to absorption in the short-wave region.

Figure 4 shows a curve obtained within the H \check{c} kel approximation with $B = -2.6$ eV. This curve is significantly different from that in Fig. 1 obtained in [31], which indicates that the Hubbard model with parameters $U \approx 7$ eV, $B \approx -1$ eV is more acceptable as compared with the model that does not take into account the ISCI.

Resuming this section, it should be noted that we have succeeded in identification of isomer of fullerene C_{90} , extracted in [31], as isomer № 6 with a symmetry of C_2 . It should be emphasized that we have succeeded to do this specifically within the Hubbard model with the following parameters: $B = -1.05$ eV and $U = 7.48$ eV.

4. Energy spectrum and optical absorption spectrum of isomer № 1 of fullerene C_{90}

Later on the investigation of isomers of fullerene C_{90} was continued in [33]. Three isomers of C_{90} were identified.

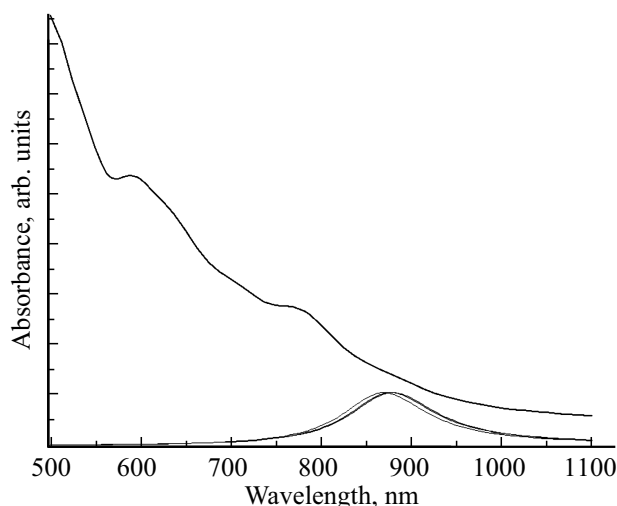


Figure 3. Demonstration of contribution of the transitions that form the absorption edge.

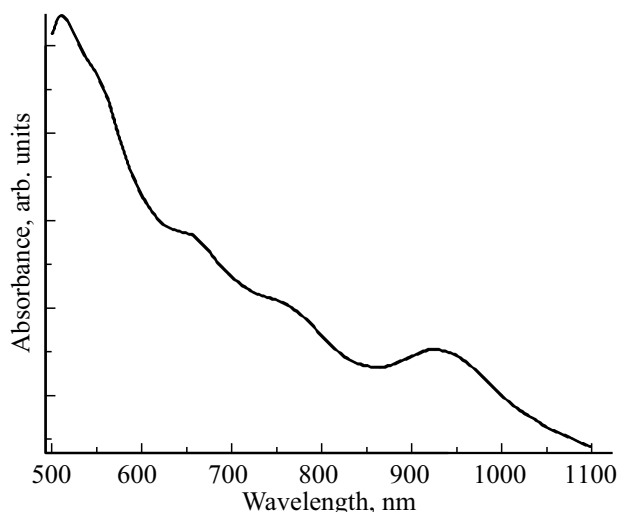


Figure 4. Optical absorption spectrum of isomer № 6 calculated within the H \check{c} kel approximation with $B = -2.6$ eV.

Optical absorption spectra of these isomers are shown in Fig. 5, which corresponds to Fig. 2 from [33]. The isomer marked as C_{90} (I) in this figure was identified by the authors of the above-mentioned study as having D_{5h} symmetry. According to [14], the isomer of C_{90} with such a symmetry is isomer № 1. Optical absorption spectrum of this isomer calculated by us within the Hubbard model is shown in Fig. 6. Before proceeding with discussion of the obtained OAS, let us take a look at the energy spectrum of the isomer in question. We have achieved the best match with experimental curve (I) in Fig. 5 at the following parameters of the Hubbard model: $U = 7.22$ eV, $B = -0.9$ eV. Table 4 shows the energy spectrum calculated at these values of parameters. The energy spectrum contains 108 levels, 54 of which are in the top Hubbard subband, and another 54 are in the bottom subband. The HOMO-LUMO

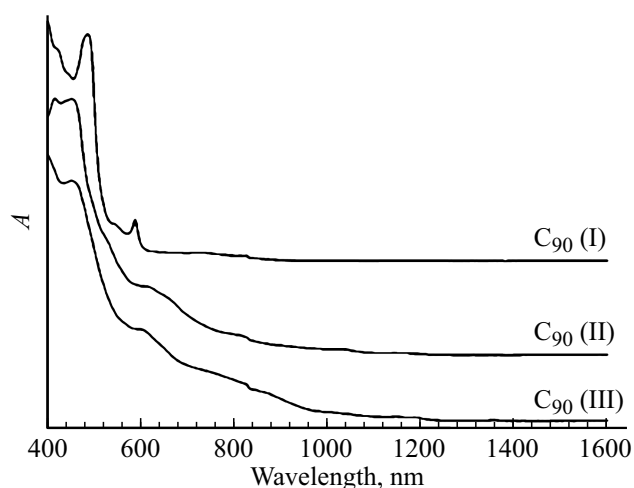


Figure 5. Experimental OAS of synthesized fullerenes (wavelengths in nanometers are plotted on the abscissa axis, absorption in relative units is plotted on the ordinate axis) [33].

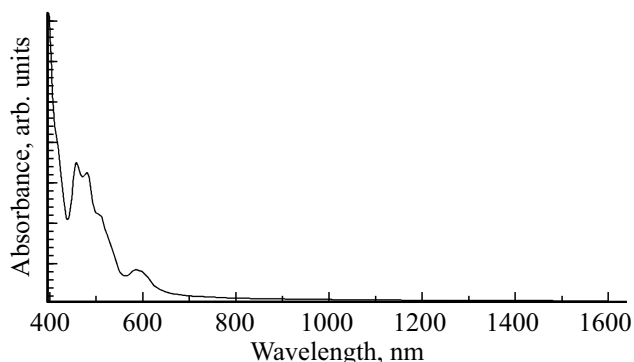


Figure 6. Optical absorption spectrum of isomer N° 1 calculated within the Hubbard model with $U = 7.22$ eV, $B = -0.9$ eV.

gap is 1.95 eV. Degeneracy of the energy levels can be 1 or 2. The symmetry group D_{5h} has eight irreducible representations: $A1'$, $A1''$, $A2'$, $A2''$, $E1'$, $E1''$, $E2'$, $E2''$. The correspondence between energy levels and irreducible representations is shown in the table. Selection rules for dipole transitions in the group D_{5h} are as follows:

$$\begin{aligned}
 &A1' \rightarrow A2'', E1' \\
 &A1'' \rightarrow A2', E1'' \\
 &A2' \rightarrow A1'', E1' \\
 &A2'' \rightarrow A1', E1'' \\
 &E1' \rightarrow A1', A2', E1'', E2' \\
 &E1'' \rightarrow A1'', A2'', E1', E2'' \\
 &E2' \rightarrow E1', E2', E2'' \\
 &E2'' \rightarrow E1'', E2', E2''
 \end{aligned}$$

The optical absorption spectrum of the isomer under consideration (Fig. 6) was obtained in accordance with these

Table 4. Energy spectrum of isomer N° 1 at $U = 7.22$ eV, $B = -0.9$ eV

-6.173, 1, A2'	-3.237, 1, A1'	1.047, 1, A2'	3.983, 1, A1''
-6.073, 2, E1'	-3.075, 2, E1'	1.147, 2, E1'	4.145, 2, E1'
-5.962, 2, E2'	-3.034, 1, A1'	1.258, 2, E2'	4.186, 1, A1'
-5.935, 2, E2''	-2.961, 2, E2''	1.285, 2, E2''	4.259, 2, E2'
-5.783, 1, A1''	-2.915, 2, E2'	1.437, 1, A1''	4.305, 2, E2''
-5.749, 2, E1''	-2.862, 2, E1''	1.471, 2, E1''	4.358, 2, E1''
-5.659, 2, E2'	-2.847, 1, A2'	1.561, 2, E2'	4.373, 1, A2'
-5.381, 2, E1'	-2.847, 2, E1''	1.839, 2, E1'	4.373, 2, E1''
-5.313, 2, E2''	-2.656, 2, E2'	1.907, 2, E2''	4.564, 2, E2'
-5.221, 2, E2'	-2.547, 2, E1'	1.999, 2, E2'	4.673, 2, E1'
-5.199, 1, A2'	-2.547, 2, E2''	2.021, 1, A2'	4.673, 2, E2''
-5.139, 2, E1''	-2.532, 2, E1'	2.081, 2, E1''	4.688, 2, E1'
-4.967, 2, E2''	-2.411, 1, A2''	2.253, 2, E2''	4.809, 1, A2''
-4.963, 2, E2'	-2.258, 2, E2''	2.257, 2, E2'	4.962, 2, E2''
-4.898, 2, E1'	-2.114, 2, E1''	2.322, 2, E1'	5.106, 2, E1'
-4.863, 1, A1'	-2.098, 2, E2'	2.357, 1, A1'	5.122, 2, E2'
-4.845, 1, A2''	-1.952, 2, E2'	2.375, 1, A2''	5.268, 2, E2'
-4.683, 2, E2'	-1.933, 1, A1'	2.537, 2, E2'	5.287, 1, A1'
-4.664, 2, E2''	-1.691, 2, E2''	2.556, 2, E2''	5.529, 2, E2''
-4.557, 2, E1'	-1.644, 2, E1'	2.663, 2, E1'	5.576, 2, E1'
-4.510, 1, A1''	-1.593, 1, A2''	2.710, 1, A1''	5.627, 1, A2''
-4.453, 2, E1''	-1.447, 2, E2'	2.767, 2, E1''	5.773, 2, E2''
-4.238, 1, A1'	-1.282, 1, A1'	2.982, 1, A1'	5.938, 1, A1'
-3.880, 2, E1''	-1.280, 2, E1''	3.340, 2, E1''	5.940, 2, E1''
-3.821, 1, A2'	-1.083, 2, E1'	3.399, 1, A2'	6.137, 2, E1'
-3.755, 2, E1'	-1.016, 1, A2''	3.465, 2, E1'	6.204, 1, A2'
-3.686, 1, A2''	-0.9100, 1, A1'	3.534, 1, A2''	6.310, 1, A1'

selection rules. The experimental curve has maxima of absorption bands at 484 and 589 nm, and the curve obtained by us has these maxima at quite close wavelengths of 470 and 589 nm. At the same time, there is a difference between experimental and theoretical curves lying in the fact that the 470 nm maximum of the theoretical curve is divided into two peaks while the experimental curve has no such a division, which may be related to measurement errors. The minimum transition frequency defined by the transition from the level of 1.047 eV ($A2'$) to the level of -0.9100 eV ($A1'$) is equal to the HOMO-LUMO gap, which corresponds to a wavelength of $\lambda = 958$ nm. Figure 7 shows OAS obtained within the Hückel approximation at $B = -2.6$ eV. The comparison of this curve with that in Fig. 5 obtained in [33] indicates a significant difference between them, which again confirms our conclusion that the Hubbard model with parameters $U = 7.22$ eV, $B = -0.9$ eV is more acceptable as compared with the model that does not take into account the ISCI.

5. Energy spectrum and optical absorption spectrum of isomers N° 16 and N° 46 of fullerene C₉₀

In addition to isomer N° 1 in [33] two more isomers were obtained. Their OAS are shown in Fig. 5 and

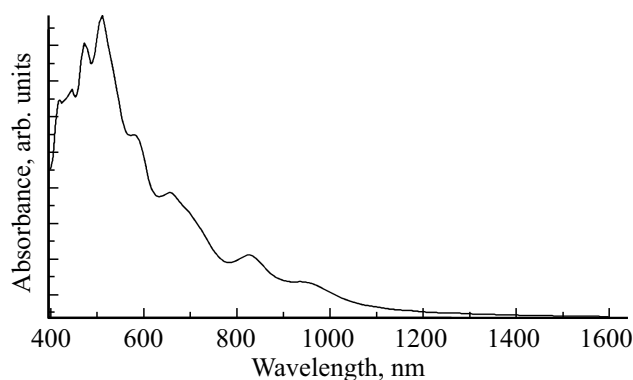


Figure 7. Optical absorption spectrum of isomer № 1 calculated within the Höckel approximation with $B = -2.6$ eV.

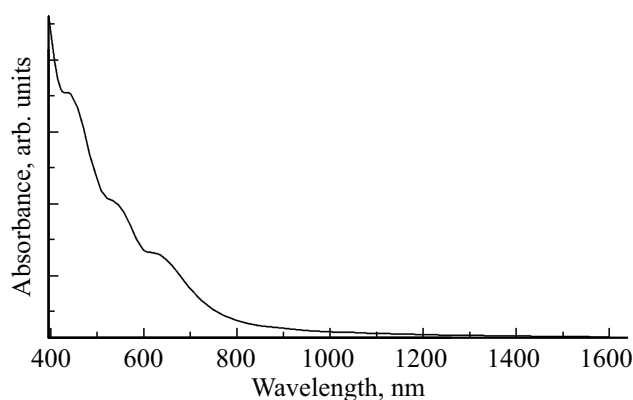


Figure 8. Optical absorption spectrum of isomer № 46 calculated within the Hubbard model with $U = 7.48$ eV, $B = -1.0$ eV.

marked as C_{90} (II) and C_{90} (III). Authors of [33] failed to identify these isomers. We compared these curves with the OAS obtained by us. The analysis has shown that the most close coincidence is observed for isomer № 46 (C_{2v}) with the curve C_{90} (II) and for isomer № 16 (C_{2v}) with the curve C_{90} (III). Figure 8 shows OAS of isomer № 46 calculated by us within the Hubbard model. Energy spectrum of this isomer for parameter values of $U = 7.48$ eV, $B = -1.0$ eV providing the best match between calculated and experimental OAS is shown in Table 5. Energies of levels are in eV, the second number in a cell is degeneracy order of the level, the third number is a symbol of irreducible representation of the level. The energy spectrum is composed of 178 levels, 89 of them are in the top Hubbard subband and the same quantity of levels are in the bottom subband. The HOMO-LUMO gap is 1.69 eV. Width of Hubbard subbands is approximately equal to 5.8 eV. The following dipole transitions are permitted in the symmetry group C_{2v} :

$$A1 \rightarrow A1, B1, B2$$

$$A2 \rightarrow A2, B1, B2$$

$$B1 \rightarrow A1, A2, B1$$

Table 5. Energy spectrum of isomer № 46 at $U = 7.48$ eV, $B = -1.05$ eV

-6.527, 1, B1	-3.306, 1, A1	0.9535, 1, B1	4.174, 1, A1
-6.489, 1, B2	-3.235, 1, A2	0.9907, 1, B2	4.245, 1, A2
-6.478, 1, A2	-3.141, 1, B2	1.002, 1, A2	4.339, 1, B2
-6.425, 1, B2	-3.122, 1, B1	1.055, 1, B2	4.358, 1, B1
-6.399, 1, B1	-3.119, 1, A2	1.081, 1, B1	4.361, 1, A2
-6.391, 1, B2	-3.106, 1, A1	1.089, 1, B2	4.374, 1, A1
-6.268, 1, A1	-3.087, 1, B1	1.212, 1, A1	4.393, 1, B1
-6.199, 1, B1	-2.977, 1, B1	1.281, 1, B1	4.503, 1, B1
-6.066, 1, A2	-2.959, 1, B2	1.414, 1, A2	4.521, 1, B2
-6.000, 1, A1	-2.849, 1, A1	1.480, 1, A1	4.631, 1, A1
-5.895, 1, B2	-2.797, 1, B1	1.585, 1, B2	4.683, 1, B1
-5.882, 1, B1	-2.740, 1, A1	1.598, 1, B1	4.740, 1, A1
-5.853, 1, B1	-2.740, 1, A2	1.627, 1, B1	4.740, 1, A2
-5.772, 1, B2	-2.740, 2, B2	1.708, 1, B2	4.740, 2, B2
-5.748, 1, A2	-2.651, 1, A2	1.732, 1, A2	4.829, 1, A2
-5.721, 1, A1	-2.611, 1, B1	1.759, 1, A1	4.869, 1, B1
-5.610, 1, B2	-2.611, 1, B2	1.870, 1, B2	4.869, 1, B2
-5.557, 1, A2	-2.607, 1, A2	1.923, 1, A2	4.873, 1, A2
-5.486, 1, B1	-2.599, 1, A1	1.994, 1, B1	4.881, 1, A1
-5.358, 1, B1	-2.295, 1, A1	2.122, 1, B1	5.185, 1, A1
-5.334, 1, B2	-2.249, 1, A2	2.146, 1, B2	5.231, 1, A2
-5.323, 1, A2	-2.215, 1, A1	2.157, 1, A2	5.265, 1, A1
-5.290, 1, A1	-2.206, 1, B2	2.190, 1, A1	5.274, 1, B2
-5.224, 1, B2	-2.195, 1, B1	2.256, 1, B2	5.285, 1, B1
-5.180, 1, A2	-2.169, 1, B1	2.300, 1, A2	5.311, 1, B1
-5.177, 1, A1	-2.118, 1, A2	2.303, 1, A1	5.362, 1, A2
-5.129, 1, A1	-2.086, 1, A1	2.351, 1, A1	5.394, 1, A1
-5.114, 1, A2	-1.983, 1, B2	2.366, 1, A2	5.497, 1, B2
-5.096, 1, B1	-1.729, 1, A2	2.384, 1, B1	5.751, 1, A2
-5.045, 1, A1	-1.700, 1, A1	2.435, 1, A1	5.780, 1, A1
-4.926, 1, B1	-1.687, 1, B2	2.554, 1, B1	5.793, 1, B2
-4.903, 1, B2	-1.657, 1, A2	2.577, 1, B2	5.823, 1, A2
-4.740, 1, A1	-1.598, 1, B2	2.740, 1, A1	5.882, 1, B2
-4.740, 1, B1	-1.591, 1, B1	2.740, 1, B1	5.889, 1, B1
-4.740, 1, B2	-1.564, 1, A1	2.740, 1, B2	5.916, 1, A1
-4.698, 1, A1	-1.264, 1, A1	2.782, 1, A1	6.216, 1, A1
-4.692, 1, A2	-1.211, 1, B1	2.788, 1, A2	6.269, 1, B1
-4.673, 1, B2	-1.210, 1, B2	2.807, 1, B2	6.270, 1, B2
-4.591, 1, B1	-1.195, 1, A1	2.889, 1, B1	6.285, 1, A1
-4.319, 1, A2	-1.177, 1, A2	3.161, 1, A2	6.303, 1, A2
-4.134, 1, A1	-0.9143, 1, B2	3.346, 1, A1	6.566, 1, B2
-3.973, 1, B2	-0.8991, 1, A1	3.507, 1, B2	6.581, 1, A1
-3.889, 1, A2	-0.8914, 1, A2	3.591, 1, A2	6.589, 1, A2
-3.723, 1, B1	-0.7400, 1, A1	3.757, 1, B1	6.740, 1, A1
-3.543, 1, B2		3.937, 1, B2	

$$B2 \rightarrow A1, A2, B2.$$

Figure 9 shows OAS of isomer № 16 obtained within the Höckel approximation with $B = -2.6$ eV. It can be seen that the spectrum differs significantly from the experimental curve.

Figure 10 shows OAS of isomer № 16 obtained from the energy spectrum calculated within the Hubbard model. Energy spectrum of this isomer for parameter values of $B = -1.0$ eV, $U = 7.2$ eV, providing the optimum match between calculated and experimental OAS, is shown in

Table 6. Energies of levels are in eV, the second number in a cell is degeneracy order, the third number is a symbol of irreducible representation of the level. The energy spectrum is composed of 180 levels, half of them lie in the top Hubbard subband, and the second half lie in the bottom subband. The HOMO-LUMO gap is equal to 1.4 eV. Width of Hubbard subbands is approximately equal to 5.8 eV. Selection rules are the same as for isomer № 16. The optical

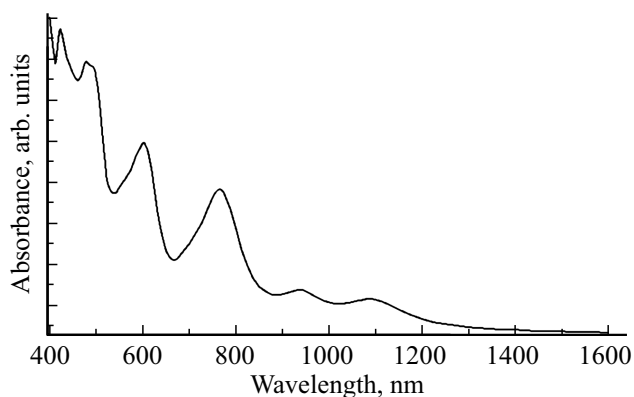


Figure 9. Optical absorption spectrum of isomer № 46 calculated within the Hückel approximation with $B = -2.6$ eV.

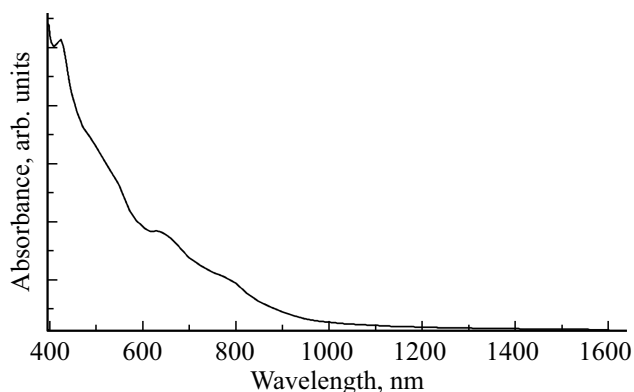


Figure 10. Optical absorption spectrum of isomer № 16 calculated within the Hubbard model with $U = 7.2$ eV, $B = -1$ eV.

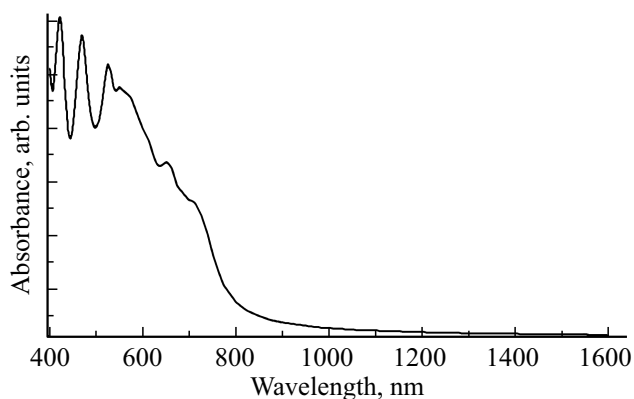


Figure 11. Optical absorption spectrum of isomer № 16 calculated within the Hückel approximation with $B = -2.6$ eV.

Table 6. Energy spectrum of isomer № 16 at $U = 7.2$ eV, $B = -1$ eV

-6.400, 1, A2	-3.071, 1, B1	0.8003, 1, A2	4.129, 1, B1
-6.387, 1, B1	-3.047, 1, B2	0.8135, 1, B1	4.153, 1, B2
-6.348, 1, B2	-3.002, 1, A1	0.8523, 1, B2	4.198, 1, A1
-6.251, 1, B2	-2.994, 1, A2	0.9486, 1, B2	4.206, 1, A2
-6.249, 1, A1	-2.951, 1, B1	0.9506, 1, A1	4.249, 1, B1
-6.138, 1, B2	-2.909, 1, A1	1.062, 1, B2	4.291, 1, A1
-6.109, 1, B1	-2.874, 1, B1	1.091, 1, B1	4.326, 1, B1
-6.033, 1, B1	-2.819, 1, B2	1.167, 1, B1	4.381, 1, B2
-6.012, 1, A1	-2.813, 1, A2	1.188, 1, A1	4.387, 1, A2
-5.995, 1, A2	-2.714, 1, B2	1.205, 1, A2	4.486, 1, B2
-5.874, 1, A2	-2.712, 1, B1	1.326, 1, A2	4.488, 1, B1
-5.732, 1, B1	-2.705, 1, A1	1.468, 1, B1	4.495, 1, A1
-5.657, 1, B2	-2.600, 1, A1	1.543, 1, B2	4.600, 1, A1
-5.606, 1, A1	-2.600, 1, A2	1.594, 1, A1	4.600, 1, A2
-5.496, 1, B2	-2.600, 1, B2	1.704, 1, B2	4.600, 1, B2
-5.450, 1, B1	-2.525, 1, B1	1.750, 1, B1	4.675, 1, B1
-5.444, 1, A1	-2.511, 1, A2	1.756, 1, A1	4.689, 1, A2
-5.418, 1, A2	-2.481, 1, B2	1.782, 1, A2	4.719, 1, B2
-5.391, 1, A2	-2.423, 1, A1	1.809, 1, A2	4.777, 1, A1
-5.298, 1, B1	-2.358, 1, A2	1.902, 1, B1	4.842, 1, A2
-5.290, 1, B2	-2.155, 1, A1	1.910, 1, B2	5.045, 1, A1
-5.130, 1, A1	-2.137, 1, B1	2.070, 1, A1	5.063, 1, B1
-5.099, 1, B2	-2.108, 1, A2	2.101, 1, B2	5.092, 1, A2
-5.070, 1, A2	-2.071, 1, A1	2.130, 1, A2	5.129, 1, A1
-5.035, 1, B1	-2.070, 1, B2	2.165, 1, B1	5.130, 1, B2
-5.023, 1, A2	-2.049, 1, B1	2.177, 1, A2	5.151, 1, B1
-4.994, 1, B2	-1.975, 1, A2	2.206, 1, B2	5.225, 1, A2
-4.992, 1, A1	-1.965, 1, B2	2.208, 1, A1	5.235, 1, B2
-4.954, 1, A1	-1.769, 1, A1	2.246, 1, A1	5.431, 1, A1
-4.879, 1, B1	-1.589, 1, A2	2.321, 1, B1	5.611, 1, A2
-4.786, 1, A2	-1.560, 1, A1	2.414, 1, A2	5.640, 1, A1
-4.770, 1, A1	-1.556, 1, B2	2.430, 1, A1	5.644, 1, B2
-4.741, 1, B2	-1.514, 1, B1	2.459, 1, B2	5.686, 1, B1
-4.703, 1, B1	-1.508, 1, B2	2.497, 1, B1	5.692, 1, B2
-4.589, 1, A1	-1.413, 1, A1	2.611, 1, A1	5.787, 1, A1
-4.580, 1, B2	-1.399, 1, A2	2.620, 1, B2	5.801, 1, A2
-4.564, 1, B1	-1.123, 1, A1	2.636, 1, B1	6.077, 1, A1
-4.485, 1, A2	-1.113, 1, B1	2.715, 1, A2	6.087, 1, B1
-4.420, 1, A1	-1.083, 1, B2	2.780, 1, A1	6.117, 1, B2
-3.912, 1, A2	-1.032, 1, A1	3.288, 1, A2	6.168, 1, A1
-3.865, 1, B1	-1.021, 1, A2	3.335, 1, B1	6.179, 1, A2
-3.849, 1, B2	-0.7861, 1, B2	3.351, 1, B2	6.414, 1, B2
-3.730, 1, A2	-0.7502, 1, A1	3.470, 1, A2	6.450, 1, A1
-3.727, 1, B2	-0.7494, 1, A2	3.473, 1, B2	6.451, 1, A2
-3.721, 1, A1	-0.6000, 1, A1	3.479, 1, A1	6.600, 1, A1

absorption spectrum shown in Fig. 10 is obtained taking into account these rules on the basis of the energy spectrum presented in Table 6. The experimental curve C₉₀ (III) (Fig. 5) demonstrates a poorly manifested maximum at 460 nm and a small plateau in the interval from 590 to 620 nm. The theoretical curve demonstrates the same diffused maximum at 440 nm and a plateau in the region from 600 to 640 nm. Both curves have a slightly noticeable swelling at 800 nm. The analysis of OAS shows that minimum absorption frequency is formed by the transition

between $[-0.6000, 1, A1]$ and $[0.8135, 1, B1]$ levels and equal to 1.41 eV, which corresponds to the absorption edge of 882 nm. It can be seen that the minimum absorption frequency is slightly different from the HOMO-LUMO of 1.4 eV. This may be related to the fact that the highest occupied level (HOMO) for this isomer is $[-0.6000, 1, A1]$, while the lowest vacant level (LUMO) is $[0.8003, 1, A2]$, but the $A1 \rightarrow A2$ transition is prohibited by the selection rules. Figure 11 shows OAS obtained within the H²ckel approximation at $B = -2.6$ eV. It can be seen that the curve differs from the experimental curve to a significant extent. Thus, we can see again that the Hubbard model with parameters $B = -1.0$ eV, $U = 7.2$ eV for isomer № 46 is more adequate as compared with the model that does not take into account the ISCI.

Conclusion

Thus, it clearly follows from the results of our study that the description of electron structure and optical absorption spectra of fullerenes must take into account the effect of intrasite Coulomb interaction of π -electrons, which is possible with the Hubbard model.

Funding

The work of M.Yu. Kokurin related to the application of linear algebra methods for the description of permitted transitions is supported by the RSF (grant No. 20-11-20085).

Conflict of interest

The authors declare that they have no conflict of interest.

References

- [1] T.O. Wehling, E. Şaçıoğlu, C. Friedrich et al. *Phys. Rev. Lett.*, **106** (23), 236805 (2011). <http://dx.doi.org/10.1103/PhysRevLett.106.236805>
- [2] R.O. Zaitsev. *JETP Lett.*, **94** (3), 206 (2011). <https://doi.org/10.1134/S0021364011150173>
- [3] J. Hubbard. *Proc. Roy. Soc.*, **276** (1365), 238 (1963). <https://doi.org/10.1098/rspa.1963.0204>
- [4] M.P. Lopez Sancho, M.C. Munoz, L. Chico. *Phys. Rev. B.*, **63** (16), 165419 (2001). DOI: 10.1103/physrevb.63.165419
- [5] T. Sagawa. *J. Phys. Soc. Jpn.*, **21** (1), 49 (1966). <https://doi.org/10.1143/JPSJ.21.49>
- [6] P.R. Wallace. *Phys. Rev.*, **71** (9), 622 (1947). <https://doi.org/10.1103/PhysRev.71.622>
- [7] J.W.G. Wilder, L.C. Venema, A.G. Rinzler, R.E. Smalley, C. Dekker. *Nature (London, UK)*, **391** (6662), 59 (1998). <https://doi.org/10.1038/34139>
- [8] H. Kuzmany, B. Burger, M. Hulman, J. Kurti, A.G. Rinzler, R.E. Smalley. *Europhys. Lett.*, **44** (4), 518 (1998). <https://doi.org/10.1209/epl/i1998-00504-y>
- [9] Ph. Kim, T.W. Odom, J.-L. Huang, Ch.M. Lieber. *Phys. Rev. Lett.* **82** (6), 1225 (1999)., <https://doi.org/10.1103/PhysRevLett.82.1225>
- [10] M.S. Dresselhaus, G. Dresselhaus, R. Saito. *Phys. Rev. B.*, **45** (11), 6234 (1992). DOI: 10.1103/PhysRevB.45.6234
- [11] M. Miao. *Carbon.*, **49** (12), 3755 (2011). <https://doi.org/10.1016/j.carbon.2011.05.008>
- [12] D.D. Michael, J.M. Alford. *Nature (London, UK)*, **393** (6686), 668 (1998). DOI: 10.1038/31435
- [13] M. Zalibera, A.A. Popov, M. Kalbac, P. Rapta, L. Dunsch. *Chem. — Eur. J.*, **14** (32), 9960 (2008). <https://doi.org/10.1002/chem.200800591>
- [14] P.W. Fowler, D.E. Manolopoulos. *An Atlas of Fullerenes* (Oxford Univ. Press, Oxford, 1995).
- [15] E.H. Lieb, F.Y. Wu. *Phys. Rev. Lett.*, **20** (25), 1445 (1968). <https://doi.org/10.1103/PhysRevLett.20.1445>
- [16] R.O. Zaitsev. *Diagram Methods in the Theory of Superconductivity and Ferromagnetism* (Editorial URSS, Moscow, 2004).
- [17] Yu.A. Izyumov. *UFN*, **169** (3), 225 (1999) (in Russian).
- [18] R.R. Nigmatulin, V.A. Toboev. *Theor. Math. Phys.*, **80** (1), 736 (1989). <https://doi.org/10.1007/BF01015312>
- [19] G.I. Mironov. *Fizika metallov i metallovedenie*, **102** (6), 611 (2006) (in Russian). <https://doi.org/10.1134/S0031918X06120039>
- [20] A.I. Murzashev. *ZhETF*, **135** (1), 122 (2009) (in Russian). DOI: 10.1134/S1063776109010142
- [21] A.I. Murzashev, Ye.O. Shadrin. *ZhETF*, **145** (6), 1161 (2014) (in Russian). DOI: 10.1134/S1063776114050148
- [22] N.V. Melnikova, A.I. Murzashev, T.E. Nazarova, E.O. Shadrin. *Synthetic Metals.*, **220**, 292 (2016). DOI: 10.1016/j.synthmet.2016.06.024
- [23] G.I. Mironov, A.I. Murzashev. *Fizika tverdogo tela*, **53** (11), 2273 (2011) (in Russian). DOI: 10.1134/S1063783411110199
- [24] A.I. Murzashev. *Izvestiya vysshikh uchebnykh zavedeniy. Fizika*, **55** (5), 49 (2012) (in Russian). DOI: 10.1007/s11182-012-9843-0
- [25] B.V. Lobanov, A.I. Murzashev. *FTT*, **55** (4), 797 (2013) (in Russian). DOI: 10.1134/S1063783413040173
- [26] A.I. Murzashev, T.E. Nazarova. *Fizika metallov i metallovedenie*, **115** (7), 675 (2014) (in Russian). DOI: 10.1134/S0031918X14040103
- [27] A.I. Murzashev, T.E. Nazarova. *ZhETF*, **146** (5), 1026 (2014) (in Russian). DOI: 10.1134/S106377611411017X
- [28] I.Ye. Kareev, V.P. Bubnov, A.I. Murzashev, B.V. Lobanov et al. *FTT*, **57** (11), 2254 (2015) (in Russian). DOI: 10.1134/S1063783415110189
- [29] A.I. Murzashev, M.Yu. Kokurin, S.K. Paimerov. *Opt. i spektr.*, **128** (9), 1238 (2020) (in Russian). DOI: 10.1134/S0030400X20090143
- [30] G.I. Mironov. *FTT*, **49** (3), 527 (2007) (in Russian). DOI: 10.1134/S1063783407030316
- [31] K. Kikuchi, N. Nakahara, T. Wakabayashi et al. *Chem. Phys. Lett.*, **188** (3–4), 177 (1992). DOI: 10.1016/0009-2614(92)90005-8
- [32] J. Elliott, P. Dawber, *Symmetry in Physics V. 1* (Mir, Moscow, 1983).
- [33] Hua Yang, Christine M. Beavers, Zhimin Wang et al. *Angew. Chem. Int. Ed.*, **49** (5), 886 (2010). DOI: 10.1002/anie.200906023